

## THE PROMPT, HIGH RESOLUTION SPECTROSCOPIC VIEW OF THE “NAKED-EYE” GRB080319B \*

V. D’ELIA<sup>1</sup>, F. FIORE<sup>1</sup>, R. PERNA<sup>2</sup>, Y. KRONGOLD<sup>3</sup>, S. COVINO<sup>4</sup>, D. FUGAZZA<sup>4</sup>, D. LAZZATI<sup>2</sup>, F. NICASTRO<sup>1</sup>, L.A. ANTONELLI<sup>1</sup>, S. CAMPANA<sup>4</sup>, G. CHINCARINI<sup>4,5</sup>, P. D’AVANZO<sup>4</sup>, M. DELLA VALLE<sup>6,11,12</sup>, P. GOLDONI<sup>7</sup>, D. GUETTA<sup>1</sup>, C. GUIDORZI<sup>4</sup>, E.J.A. MEURS<sup>8,9</sup>, E. MOLINARI<sup>4</sup>, L. NORCI<sup>9</sup>, S. PIRANOMONTE<sup>1</sup>, L. STELLA<sup>1</sup>, G. STRATTA<sup>10</sup>, G. TAGLIAFERRI<sup>4</sup>, P. WARD<sup>8</sup>.

*Draft version May 2, 2019*

### ABSTRACT

GRB080319B reached 5th optical magnitude during the burst. Thanks to the VLT/UVES rapid response mode, we observed its afterglow just 8m:30s after the GRB onset when the magnitude was  $R \sim 12$ . This allowed us to obtain the best signal-to-noise, high resolution spectrum of a GRB afterglow ever (S/N per resolution element  $\sim 50$ ). The spectrum is rich of absorption features belonging to the main system at  $z=0.937$ , divided in at least six components spanning a total velocity range of 120 km/s. The VLT/UVES observations caught the absorbing gas in a highly excited state, producing the strongest Fe II fine structure lines ever observed in a GRB. A few hours later the optical depth of these lines was reduced by a factor of 4-20, and the optical/UV flux by a factor of  $\sim 60$ . This proves that the excitation of the observed fine structure lines is due to “pumping” by the GRB UV photons. A comparison of the observed ratio between the number of photons absorbed by the excited state and those in the Fe II ground state suggests that the six absorbers are  $\gtrsim 18 - 34$  kpc from the GRB site, with component I  $\sim 2$  times closer to the GRB site than components III to VI. Component I is characterized also by the lack of Mg I absorption, unlike all other components. This may be due to a higher gas temperature, suggesting a structured ISM in this galaxy complex.

*Subject headings:* Gamma Ray Bursts

### 1. INTRODUCTION

For a few hours after their onset, Gamma Ray Burst (GRB) afterglows are the brightest beacons in the far Universe. In a small fraction of the cases, extremely bright optical transient emission is associated with the GRB event, offering a superb opportunity to investigate high- $z$  galaxies through high resolution spectroscopy of the optical transient. The study of the rich absorption spectra can yield unique information on the gas in the GRB environment and the physical, chemical and dy-

namical state and geometry of the inter-stellar matter (ISM) of intervening galaxies, including the GRB host galaxy.

GRB080319B was discovered by the Burst Alert Telescope (BAT) instrument on board Swift on 2008, March 19, at 06:12:49 UT. Swift slewed to the target in less than 1 minute and bright afterglows were found by both the X-Ray Telescope (XRT) and UV-Optical Telescope (UVOT) at RA = 14h 31m 40.7s, Dec = +36° 18’ 14.7” (Racusin et al. 2008a) with observations starting 60.5 and 175 s after the trigger, respectively. The field of GRB080319B was imaged by the “Pi of the Sky” apparatus located at Las Campanas Observatory before, during and after the GRB event (Cwiok et al. 2008). The field was also targetted by the robotic telescope REM just 43 s after the BAT trigger (Covino et al. 2008a, b). The TORTORA wide-field optical camera (12 cm diameter, 20×25 deg FOV, TV-CCD, unfiltered) mounted on REM imaged, with good temporal resolution, the field before, during and after the GRB event (Karpov et al. 2008). These observations show that the GRB reached the magnitudes  $R = 5$  about 20 s and  $H = 4.2$  about 50 s after the trigger. This makes GRB080319B the brightest GRB ever recorded at optical wavelengths (Bloom et al. 2008, Racusin et al. 2008b).

The optical afterglow of GRB080319B was observed at high resolution with VLT/UVES starting just 8m:30s after the BAT trigger, thanks to the VLT rapid response mode (RRM), when its magnitude was  $R \sim 12 \div 13$ . This allowed us to obtain the best signal-to-noise, high resolution spectrum of a GRB afterglow ever (S/N per resolution element  $\sim 50$ ). Two further RRM and target of opportunity (ToO) observations were obtained 2 – 3 hours after the event. Several absorption systems are

\*BASED ON OBSERVATIONS COLLECTED AT THE EUROPEAN SOUTHERN OBSERVATORY (ESO) WITH THE VLT/KUEYEN TELESCOPE, PARANAL, CHILE, IN THE FRAMEWORK OF PROGRAM 080.A-0398.

Electronic address: delia@oa-roma.inaf.it

<sup>1</sup> INAF-Osservatorio Astronomico di Roma, via Frascati 33, Monteporzio (Rm), I00040, Italy;

<sup>2</sup> JILA and Department of Astrophysical and Planetary Science, CU Boulder, Boulder, 80309, USA;

<sup>3</sup> Instituto de Astronomia, Universidad Nacional Autonoma de Mexico, Apartado Postal 70-264, 04510 Mexico DF;

<sup>4</sup> INAF, Osservatorio Astronomico di Brera, via E. Bianchi 46, 23807 Merate (LC), Italy;

<sup>5</sup> Universita’ di Milano Bicocca, Piazza della Scienza 3, 20126 Milano, Italy

<sup>6</sup> INAF, Osservatorio Astronomico di Capodimonte, Napoli, Italy;

<sup>7</sup> APC/UMR 7164, Service d’Astrophysique, CEA Centre de Saclay;

<sup>8</sup> School of Cosmic Physics, DIAS, 31 Fitzwilliam Place, Dublin 4, Ireland;

<sup>9</sup> School of Physical Sciences, DCU, Glasnevin, Dublin 9, Ireland;

<sup>10</sup> ASI Science Data Center, via Galileo Galilei, 00044 Frascati, Italy.

<sup>11</sup> ESO, Karl-Schwarzschild-Strasse 2, D-85748 Garching bei Munchen

<sup>12</sup> International Center for Relativistic Astrophysics Network, Piazzale Repubblica 10, Pescara

TABLE 1  
GRB080319B journal of observations

Observation	UT observation	Time from burst (s)	Exposure (s)	S/N range	Dichroics	Arms	Afterglow R mag
UVES RRM 1	2008 Mar 19, 06:21:26	517	600	30 ÷ 50	2	Blue + Red	12 ÷ 13
UVES RRM 2	2008 Mar 19, 08:06:42	6833	1800	7 ÷ 12	1 + 2	Blue + Red	16 ÷ 17
UVES ToO	2008 Mar 19, 09:07:22	10482	1200	5 ÷ 8	1 + 2	Blue + Red	16 ÷ 17

present in these spectra. Vreeswijk et al. (2008) identify the highest redshift system at 0.937 as the GRB host galaxy.

This letter concentrates on the analysis of fine structure lines associated with the main system at  $z=0.937$  and on their variability. Section 2 describes the datasets and data analysis; Section 3 presents the UVES spectroscopy and discusses the absorption features and their variability; our conclusions are given in Section 4. A  $H_0 = 70 \text{ km s}^{-1} \text{ Mpc}^{-1}$ ,  $\Omega_M=0.3$ ,  $\Omega_\Lambda = 0.7$  cosmology is adopted throughout.

## 2. OBSERVATIONS AND DATA ANALYSIS

We observed the bright afterglow of GRB080319B in the framework of the ESO program 080.A-0398 with the VLT/UVES (Dekker et al. 2000). Observation Log is reported in Table 1. Both UVES dichroics, as well as the red and the blue arms, were used.

The first, 10min observation, was performed in RRM and started just 8m:30s after the GRB event, when the afterglow was extremely bright ( $R=12-13$ ). This afforded a  $S/N=30 \div 50$  per resolution element. Two more UVES observations followed, the first one again in RRM mode, activated in the framework of program 080.D-0526 and starting 1.9 hours after the GRB event, and the second a ToO, starting 2.9 hours after the GRB, see Table 1.

Data reduction was carried out by using the UVES pipeline (Ballester et al. 2000). The final useful spectra extend from  $\sim 3800 \text{ \AA}$  to  $\sim 9500 \text{ \AA}$ . The resolution element, set to two pixels, ranges then from  $4 \text{ km s}^{-1}$  at  $4500 \text{ \AA}$  to  $1.9 \text{ km s}^{-1}$  at  $9000 \text{ \AA}$ . The noise spectrum, used to determine the errors on the best fit line parameters, was calculated from the real-background-subtracted spectra using line-free regions. This takes into account both statistical and systematic errors in the pipeline processing and background subtraction.

## 3. UVES SPECTROSCOPY OF FINE STRUCTURE LINES

The three UVES observations were analyzed in the MIDAS environment using the FITLYMAN procedure (Fontana & Ballester 1995). The highest  $z$  system present in these spectra is at  $z=0.937$ , as also reported by Vreeswijk et al. 2008. This system presents absorption features from the ground states of MgI, MgII, FeII and several FeII fine structure lines (FeII\* hereafter). The most striking feature in the UVES spectra is the variation of the opacity of the fine structure lines between the first and the second UVES observations. Fig. 1 shows the Fe II $\lambda$ 2374 and Fe II\* $\lambda$ 2396 absorption features in the three epochs. We see strong variations of both lines. While the strength of the Fe II $\lambda$ 2374 absorption increases from the first to the third epoch, strong Fe II\* $\lambda$ 2396 absorption is present only in the first spectrum and nearly disappears in the second and third spectra. The huge variations of Fe II fine structure lines imply that “pumping” by the GRB UV photons is the main mechanism

for populating the excited states (Silva & Viegas 2002; Prochaska et al. 2006; Vreeswijk et al. 2007).

UVES spectra of bright GRB afterglows have always revealed a complex structure of the absorption system associated with the GRB host galaxy, reflecting the clumpy nature of the ISM (see e.g. D’Elia et al. 2007). This is confirmed by the UVES spectra of GRB080319B. A detailed line fitting was performed using a Voigt profile with three parameters: the line wavelength, column density and Doppler parameter  $b$ . Several absorption features were fitted simultaneously by keeping the redshift and  $b$  value of each component fixed at their common values (best fit  $b$  values in the  $3 \div 10$  range). The Fe II\* $\lambda$ 2396 absorption lines are not saturated, and can be used to guide the identification of different components. Statistically acceptable fits to the first epoch UVES spectrum, are obtained by using six components. These span a range of  $\sim 120 \text{ km/s}$  in velocity space. Fig. 2 shows the best fitting model to the Mg I $\lambda$ 2026, Fe II $\lambda$ 2382 and Fe II\* $\lambda$ 2396 lines. The lower S/N spectra from the second and third epochs were then fitted by fixing the  $z$  and  $b$  parameters of each component at their respective best fit values found for the first epoch, highest S/N spectrum. Table 2 gives the Mg I, Fe II and Fe II\* column densities of each of the six components in the three epochs. Components are labeled from I to VI for decreasing wavelengths (and decreasing redshift, or positive velocity shift with respect to a zero point, arbitrarily placed at  $z=0.9371$ ). The second column indicates which transitions have been used to evaluate the column density of each ionic specie. Strong Mg II absorption is present for all components, but reliable column densities cannot be derived for this ion because the lines are strongly saturated. The column density uncertainties are given at the  $1\sigma$  confidence level, while upper limits are at a 90% confidence level (i.e.  $1.6\sigma$ ). The column densities derived from the second epoch spectrum are always consistent with those derived from the third epoch spectrum, to within their relatively large errors. Thus, in order to improve the  $S/N$ , we also added together the second and third epoch spectra and repeated the fits.

Mg I is detected for all components but I. The Mg I column density of the five components is consistent with a constant value at all epochs. Conversely we see strong variations of both Fe II fine structure and ground state lines for all six components. The Fe II fine structure lines of the lower redshift components underwent the strongest variations, as most of these lines are not detected in the second and third epoch spectra. The Fe II fine structure lines of the highest redshift component I vary less, and they are still detected in the second and third epoch spectra. Fig. 3 compares the column density of the Fe II\* $\lambda$ 2396 line of the six components in the first epoch spectrum to that measured 2-3 hr later. The column density of component I dropped by a factor of  $\sim 4$ , while that of component III dropped by a factor of

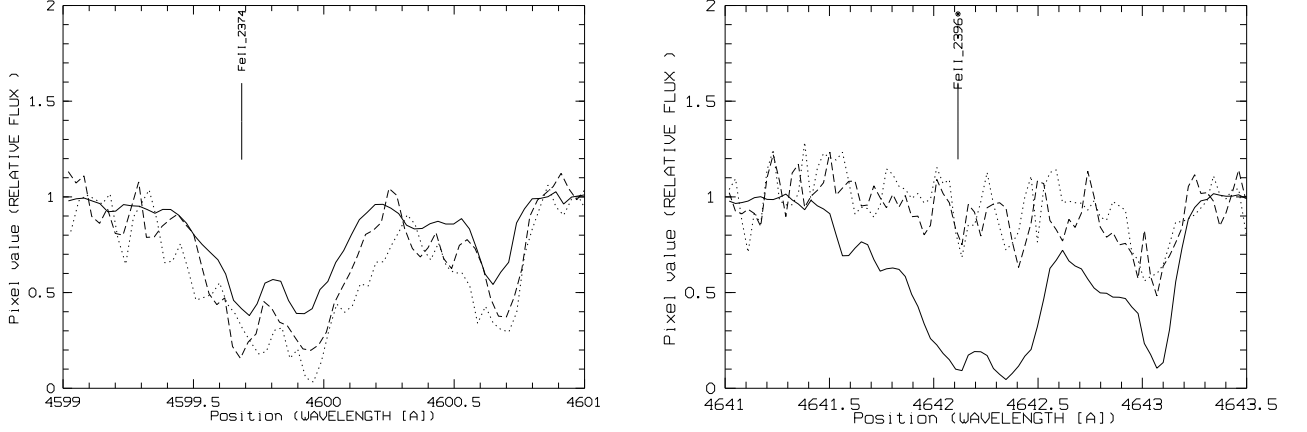


FIG. 1.— The UVES spectra of GRB080319B around the Fe II  $\lambda$ 2374 (left panel), and Fe II\*  $\lambda$ 2396 (right panel) transitions. Solid lines refer to the first epoch spectrum (8m30s after the Swift trigger), dashed lines refer to the second epoch spectrum (1.9 hours after the GRB event), and dotted lines refer to the the third epoch spectrum (2.9 hours after the GRB event).

$\sim 20$  (Table 3). On the other hand, the column density of ground state Fe II increased by a factor of 1.3-2 for all six components (Table 3). The de-excitation of fine structure levels into ground state levels, as time passes and the UV radiation field diminishes, is certainly contributing to this increase. For all components, the increase in the column density of the Fe II resonant line is consistent with the decrease of the fine structure lines within  $1.5\sigma$ . This is a first indication that the absorbing medium must be relatively distant, since photoionization of the medium by the burst photons, predicted to be important in the vicinity of the source (Perna & Loeb 1998; Perna & Lazzati 2002) appears to be negligible here.

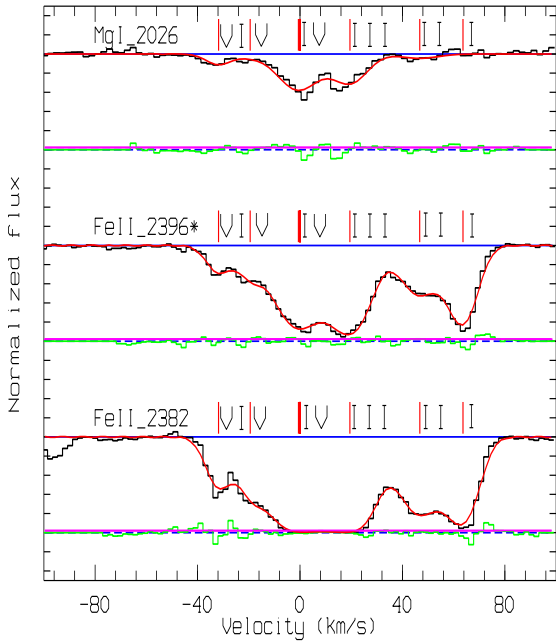


FIG. 2.— The first UVES spectrum of GRB080319B around the Fe II  $\lambda$ 2382, Fe II\*  $\lambda$ 2396\* and Mg I  $\lambda$ 2026 transitions. The solid line shows the six component fit (I to VI from higher to lower redshift). The velocity position of the components is marked with vertical lines.

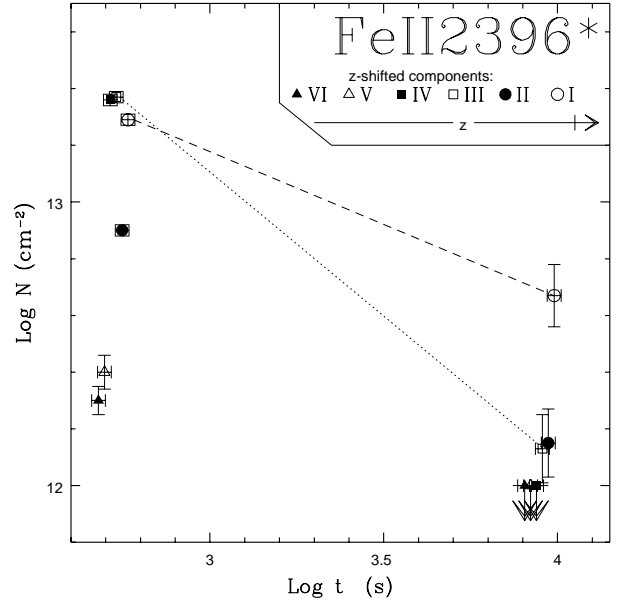


FIG. 3.— The column density of the Fe II  $\lambda$ 2396\* line for the six components as a function of time. For clarity reasons, components have been slightly shifted with each other. Late time points represent the observations 2 and 3 added together. Note that the highest redshift component I varies less than the lower redshift components III and IV (the dashed and dotted lines are for components I and III, respectively).

#### 4. DISCUSSION AND CONCLUSIONS

Prompt, time resolved, high resolution spectroscopy of the bright optical/UV afterglow of GRB080319B confirms the power of this tool for dissecting the ISM of high- $z$  galaxies. Thanks to the VLT RRM, which allowed the observation of the target in just 5min (rest frame), we were able to catch the absorbing gas in a highly excited state, producing the strongest Fe II fine structure lines ever observed in a GRB (or QSO) spectrum. The optical depth of these lines was dramatically reduced 2-3 hours later, implying a factor of 4-20 decrease for all six components belonging to the main absorption system. At the same time, the optical/UV flux dropped

TABLE 2  
MgI, FeII and FeII\* column densities for the six components at three epochs.

Specie	Transition	Obs.	I (64 km/s)	II (47 km/s)	III (20 km/s)	IV (0 km/s)	V (-20 km/s)	VI (-32 km/s)	
Mg I	$\lambda 2026$	1	< 11.80	$12.14 \pm 0.10$	$13.00 \pm 0.02$	$13.18 \pm 0.01$	$11.83 \pm 0.17$	$12.38 \pm 0.05$	
	$\lambda 2852$	2	< 11.2	$12.09 \pm 0.03$	$13.06 \pm 0.08$	$12.94 \pm 0.12$	$11.77 \pm 0.06$	$12.02 \pm 0.05$	
		3	< 11.6	$12.05 \pm 0.04$	$13.39 \pm 0.11$	$12.87 \pm 0.10$	$11.81 \pm 0.07$	$12.05 \pm 0.07$	
		2+3	< 11.0	$12.08 \pm 0.02$	$13.18 \pm 0.06$	$12.95 \pm 0.07$	$11.80 \pm 0.05$	$12.07 \pm 0.05$	
FeII	$\lambda 2374$	1	$13.52 \pm 0.01$	$13.11 \pm 0.02$	$13.84 \pm 0.02$	$13.79 \pm 0.02$	$12.76 \pm 0.02$	$12.77 \pm 0.02$	
	$\lambda 2382$	2	$13.78 \pm 0.05$	$13.26 \pm 0.09$	$14.13 \pm 0.05$	$14.01 \pm 0.06$	$13.11 \pm 0.06$	$12.86 \pm 0.22$	
		3	$13.99 \pm 0.07$	$13.19 \pm 0.17$	$14.32 \pm 0.10$	$13.99 \pm 0.11$	$12.77 \pm 0.85$	$12.81 \pm 0.34$	
		2+3	$13.87 \pm 0.04$	$13.24 \pm 0.10$	$14.19 \pm 0.08$	$14.00 \pm 0.10$	$13.00 \pm 0.12$	$12.84 \pm 0.17$	
FeII*	$\lambda 2333$	1	$13.29 \pm 0.02$	$12.90 \pm 0.02$	$13.37 \pm 0.02$	$13.36 \pm 0.02$	$12.40 \pm 0.06$	$12.30 \pm 0.05$	
	$\lambda 2365$	2	$12.66 \pm 0.05$	$12.33 \pm 0.04$	< 12.2	< 12.2	< 12.2	< 12.2	
		$\lambda 2389$	3	$12.66 \pm 0.11$	< 12.6	< 12.6	< 12.6	< 12.6	< 12.6
		$\lambda 2396$	2+3	$12.67 \pm 0.11$	$12.15 \pm 0.12$	$12.13 \pm 0.12$	< 12.0	< 12.0	< 12.0
FeII**	$\lambda 2328$	1	$13.03 \pm 0.01$	$12.53 \pm 0.01$	$13.20 \pm 0.01$	$13.16 \pm 0.01$	$12.45 \pm 0.01$	$11.78 \pm 0.27$	
		2	< 13.0	< 13.0	< 13.0	< 13.0	< 13.0	< 13.0	
		3	< 13.4	< 13.4	< 13.4	< 13.4	< 13.4	< 13.4	
		2+3	< 12.8	< 12.8	< 12.8	< 12.8	< 12.8	< 12.8	
FeII***	$\lambda 2338$	1	$12.86 \pm 0.02$	$12.48 \pm 0.04$	$13.02 \pm 0.02$	$13.02 \pm 0.02$	$11.89 \pm 0.13$	$11.82 \pm 0.13$	
		$\lambda 2359$	2	< 13.0	< 13.0	< 13.0	< 13.0	< 13.0	< 13.0
			3	< 13.4	< 13.4	< 13.4	< 13.4	< 13.4	< 13.4
			2+3	< 12.8	< 12.8	< 12.8	< 12.8	< 12.8	< 12.8
FeII****	$\lambda 2345$	1	$12.54 \pm 0.02$	$12.24 \pm 0.04$	$12.79 \pm 0.02$	$12.76 \pm 0.02$	$11.78 \pm 0.37$	$11.70 \pm 0.10$	
		$\lambda 2414$	2	< 12.7	< 12.7	< 12.7	< 12.7	< 12.7	< 12.7
			3	< 13.1	< 13.1	< 13.1	< 13.1	< 13.1	< 13.1
			2+3	< 12.5	< 12.5	< 12.5	< 12.5	< 12.5	< 12.5

All values are logarithmic  $\text{cm}^{-2}$

TABLE 3  
The Fe II and Fe II\* column density ratios between observation 1 and 2+3.

	I	II	III	IV	V	VI
Fe II	$-0.35 \pm 0.05$	$-0.13 \pm 0.12$	$-0.35 \pm 0.10$	$-0.21 \pm 0.12$	$-0.24 \pm 0.14$	$-0.07 \pm 0.19$
Fe II*	$0.62 \pm 0.13$	$0.75 \pm 0.14$	$1.24 \pm 0.14$	> 1.36	> 0.40	> 0.30

Ratios are expressed in logarithmic  $\text{cm}^{-2}$

by a factor of  $\sim 60$  (Bloom et al. 2008, Racusin et al. 2008b). The variation of the Fe II fine structure lines is spectacular, when compared to previous GRB observations. Before GRB080319B, the best case was certainly that of GRB060418 at  $z=1.490$ , observed with UVES on comparably short timescales. Vreeswijk et al. (2007) report for this burst variations of the Fe II fine structure lines column densities by a factor of 1.4, in spectra taken 700 s and 7680 s after the GRB onset; in the same time interval the optical/UV flux dropped by a factor of  $\sim 20$ . The variations seen in GRB080319B at similar rest frame timescales are clearly much more prominent. This is probably due to the extremely intense optical/UV radiation field of GRB080319B.

The optical GRB magnitude reached  $V \sim 6$  about 40 s after the start of the GRB event. At  $z=0.937$ , this magnitude implies a  $\sim 912\text{\AA}$  ionizing luminosity  $L = 1.2 \times 10^{51}$  erg  $\text{s}^{-1}$ , assuming a power law spectrum with frequency spectral index  $-1$  and integrating it up to 1 keV. Since the Fe II ionization potential is just above the photoionization edge of H, this ion is efficiently screened and it can be photoionized only after H has been photoionized. An order of magnitude estimate for the maximum H photoionization radius is given by  $R = \sqrt{\frac{N_\gamma \sigma_H}{4\pi}}$  cm, where  $N_\gamma$  is the number of photoionizing photons at 13.6 eV, and  $\sigma_H = 8 \times 10^{-18}$   $\text{cm}^2$  is the H photoionization cross

section. We can compute the number of ionizing photons by integrating the optical/UV light curve (Bloom et al. 2008, Racusin et al. 2008b). We find  $N_\gamma = 8.6 \times 10^{62}$  ph at  $912\text{\AA}$ ; similar numbers are obtained by extrapolating the XRT X-ray spectrum down to  $912\text{\AA}$  assuming no absorption, in addition to the galactic value, along the line of sight. This yields an upper limit to the H photoionization radius  $\lesssim 7.5$  kpc. At distances larger than this, H must be neutral, and Fe II will not be fully photoionized. Note that the maximum photoionization radius of Mg I is comparable to that of H. With a photoionization cross section of  $1.7 \times 10^{-18}$   $\text{cm}^2$  and an ionization potential of 7.64 eV, the ionization radius of Mg I is  $\sim 4.6$  kpc. These estimates are confirmed by time evolving photoionization calculations using the observed GRB light-curve to estimate the input photoionization and assuming an optically thin medium (radiative transfer is neglected in this first approximation calculation). On the other hand, if radiative transfer in a medium of density  $n_H$  were included, the upper limit to the photoionization radius would be given by  $R = \frac{3 \times N_\gamma}{4\pi n_H}^{1/3}$  cm, which gives  $R > 190(n_H/\text{cm}^{-3})^{-1/3}$  pc.

A constraint on the distance of the absorbing gas to the GRB can be obtained using the ratio between the number of photons absorbed by the excited state and the Fe II ground state. This ratio in the prompt spec-

trum of GRB080319B is 0.6 for component I and II, between 0.3 and 0.4 for components III, IV, V and VI. Note that the value for component I and II is close to the maximum theoretical value of 0.8. As a comparison, the same ratio in the prompt spectrum of GRB060418 was 0.09 (Vreeswijk et al. 2007). Calculations of population ratios (Silva & Viegas 2002; see also Prochaska, Chen & Bloom 2006) show that the observed ratios are obtained for a UV flux of  $\sim 3 \times 10^6 - 10^7 G_0$  for the six components, where  $G_0 = 1.6 \times 10^{-3} \text{ erg cm}^{-2} \text{ s}^{-1}$ . This implies distances from the GRB to the six absorbers  $R = [L_{UV}/(4\pi G_0 \times (3 \times 10^6 - 10^7))]^{1/2} \approx 18 - 34 \text{ kpc}$  (having assumed  $L_{UV} = 6.7 \times 10^{50} \text{ erg s}^{-1}$ ). Taken at face value, these distances are larger than the size of a typical galaxy at  $z \sim 1$  (e.g. Sargent et al. 2007) and would imply that the 0.937 system is in the outskirts of the GRB host galaxy or in a nearby clump along the line of sight. Interestingly, HST imaging of the field show diffuse emission elongated south of the afterglow. In particular, two faint clumps of emissions are located at  $1.5''$  and  $3''$  from the afterglow (Tanvir et al. 2008). At  $z=0.937$  these correspond to projected distances of 12 and 24kpc, and may suggest the presence of a complex structure of clumps around the GRB site. If this is the case, the absorbers may well belong to one of these clumps.

Component I has the highest ratio of photons absorbed by Fe II excited and ground state, suggesting that this component is the closest one to the GRB site. Note that

this component shows Fe II fine structure line variations significantly smaller than the other components (viz. III and IV, Fig. 3 and Table 3). The decay time of the first excited state ( $\sim 500 \text{ s}$ , Vreeswijk et al. 2007) is shorter than or comparable to the rest frame time between the first and second epoch spectra. This implies that it is easier to maintain a high level of excitation for a longer time for an absorber closer to the source of UV photons than for farther absorbers, in agreement with our previous results. Alternatively, collisional excitation may help in maintaining a sizeable population of excited levels in this component. Component I does not show strong Mg I absorption, unlike all other components. Both analytical and time evolving photoionization calculations show that Mg I should be present at distances  $> 10 \text{ kpc}$ , where the analysis of the fine structure lines suggest that also component I is located. The lack of Mg I in component I can be explained by a gas temperature  $> 5 \times 10^4 \text{ K}$  (Shull & Van Steenberg 1982), while the temperature of the gas of the other components should be lower than this value. This is a further confirmation that the ISM of high- $z$  galaxies is complex, structured and characterized by numerous distinct components with different temperature and (most likely) density.

We acknowledge support from ASI/INAF contracts ASI/I/R/039/04 and ASI/I/R/023/05/0.

#### REFERENCES

- Ballester, P., Modigliani, A., Boitquin, O. et al. 2000, ESO Messenger, 101, 31  
 Bloom, J.S., Perley, D., A., Li, W. et al. 2008, ApJ submitted, astro-ph/0803.3215  
 Covino, S. et al., 2008a, GCN 7431  
 Covino, S. et al., 2008b, GCN 7446  
 Cwiok, M. et al. 2008, GCN 7439  
 Dekker, H., D'Odorico, S., Kaufer, A., Delabre, B., Kotzlwski, H., 2000, SPIE, 4008, 534  
 D'Elia, V., Fiore, F., Meurs, E.J.A. et al., 2007, 467, 629  
 D'Odorico, V., Cristiani, S., Romano, D., Granato, G., & Danese, L. 2004, MNRAS, 424, 23  
 Fontana, A. & Ballester, P. 1995, The ESO Messenger, 80, 37  
 Karpov et al. 2008, GCN 7452  
 Perna, R. & Loeb, A. 1998, ApJ, 501, 467  
 Perna, R. & Lazzati, D. 2002, ApJ, 580, 261  
 Prochaska, J. X., Chen, H.-W., & Bloom, J. S. 2006, ApJ, 648, 95  
 Racusin, J.L. et al. 2008a GCN 7427  
 Racusin, J.L. et al. 2008b, in preparation  
 Sargent, M.T., Carollo, C.M., Lilly, S.J. et al. 2007, ApJS, 172, 434  
 Shull, J.M., van Steenberg, M. 1982, ApJS, 48, 95  
 Silva, A.I., & Viegas, S.M. 2002, MNRAS, 329, 135  
 Tanvir, N.R. et al. 2008, GCN 7569  
 Vreeswijk, P.M. et al. 2007, A&A, 468, 83  
 Vreeswijk, P.M. et al. 2008, GCN 7451